

Decoupling Control and Simulation of a 3-RSR Spheroid Parallel Wrist

Cai Xiao, Hao Jiang, Guo Ying Zhang, Tao Zhang*, Yisheng Guan* and Guanfeng Liu

*Biomimetic and Intelligent Robotics Lab(BIRL),School of Electromechanical Engineering
Guangdong University of Technology
Guangzhou, Guangdong Province China, 510006.*

Abstract—The control of position and trajectory tracking are critical issues in parallel robots. Traditional PID tracking algorithms, which are based on kinematics control use the position and speed deviation as a negative feedback in order to design a controller. However, this method is not only hard to maintain the excellent dynamic and static quality of a system, but it is also incapable of realizing complete decoupling, and it needs large energy to be controlled. To overcome such drawbacks, this paper proposes, a computed torque decoupling control strategy for a 3-RSR spheroid parallel mechanism. The control strategy includes a computed torque decoupling control method with traditional PD controller and self-adaption fuzzy controller. It was proved that the corresponding Lyapunov function is global asymptotic stable in the ideal and non-ideal estimation. A set of ADAMS-MATLAB dynamic simulations were established based on virtual prototyping technology. The results demonstrated that the performance of the control scheme with self-adaption fuzzy controller is more effective than that with PD controller.

Index Terms—Parallel robot dynamic, PID, Computed torque decoupling control.

I. INTRODUCTION

In general, parallel robots consist of two platforms and several links, one platform is designed as static and the other as dynamical. This design results in a closed-loop kinematic chain mechanism, which feature represents the most significant difference between serial and parallel robots [1], [2], [3]. Parallel robots have several advantages compared to serial ones, including high pay-load/weight ratio, high velocity, high accuracy, high stiffness, and low inertia. Lower mobility parallel robots are one of the hotspots in current research of robotic mechanisms. Compared to their 6-DOF counterpart, parallel mechanisms with lower-mobility have the advantages of simple architecture and lower manufacturing

*Corresponding authors, tzhang@gdut.edu.cn, ysguan@gdut.edu.cn. The work in this paper is partially supported by the Natural Science Foundation of China (Grant No. 51905105), the Natural Science Foundation of Guangdong (Grant No. 2015A030308011), and the Frontier and Key Technology Innovation Special Funds of Guangdong (Grant No. 2016B090911002, 2017B090910008, 2017B090910002), and the Guangdong Yangfan Program for Innovative and Entrepreneurial Teams (Grant No. 2017YT05G026), and the Natural Science Foundation of Guangdong Province-Regular Project(Design theory and method of cable-driven flexible andromorphic limb with variable stiffness).

costs. Meanwhile, they are suitable for many tasks that require less than 6-DOF. A three degrees of freedom 3-RSR spheroid parallel wrist (SPW) has been proposed in the literature [4], which can be used as a wrist at the end of Delta or selective compliance assembly robot arm (SCARA) robots. Such hybrid robots can be used in electronic and light industries, where large changes in object configuration, in terms of orientation and position, need to be performed.

However, similar to traditional parallel mechanisms, the 3-RSR SPW suffers from strong coupling and nonlinear characteristics, which make it challenging to control the robot, especially, when high-speed and highly accurate in position and trajectory tracking control are required [5].

In order to solve such problems, several control approaches have been proposed, including nonlinear potential difference (PD) control [6], self-tuning adaptive control [7], neural network control [8], adaptive synchronized control [9], and proportionalintegral (PI)-type synchronized control [10]. However, these methods have difficulty in accurately controlling nonlinear and strongly coupled systems of parallel robots. In this paper, a computed torque decoupling control strategy is proposed, where a nonlinear compensator is introduced into the internal control loop, and the complex nonlinear and strongly-coupled control system is transformed into an easy-to-control linear constant system. The 3-RSR SPW robot prototype is shown in Fig. 1. Simulation results have shown that its performance is satisfactory.

This paper is organized as follows. In Section II, a dynamic model of 3-RSR SPW is established and its Jacobian matrices are deduced. In Section III, the decoupling control system based on a PD controller and a self-adaption PD controller is briefly introduced. In Section IV, a simulation platform is developed and the control effect of the PD controller and the self-adaption PD controller is analyzed. Finally, the conclusions of this study are drawn in Section V.

II. DYNAMIC MODELING OF 3-RSR SPW

A. Dynamic Model

The following assumptions and simplifications have been made, since they have less impact on the model [11]:

- 1) No joint friction and clearance;

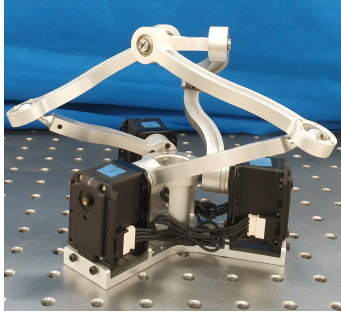


Fig. 1. The 3-RSR SPW prototype

- 2) The master and passive links as straight link;
- 3) Considering that the driven link does not play a leading role in the dynamics of the mechanism, the mass of driven link was divided between two parts.

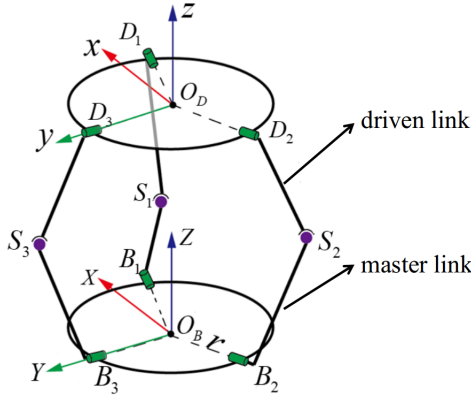


Fig. 2. The simplified 3-RSR SPW mechanism

As it can be seen in Fig. 2, the coordinate system O_Dxyz is fixed on the moving platform, D_i are revolute joints of the moving platform, S_i are spherical joints, B_i are revolute joints of the base platform, r is the radius of the moving and static platforms, and the coordinate system O_BXYZ is fixed on the base platform (where $i = 1, 2, 3$).

The kinetic energy of the master link equals its own kinetic energy and the kinetic energy from the coupled driven link. The link mass reassignment makes the centroid re-measurement. The centroid of the master link, calculated by resultant torque principle is zero [12]. In the case of not specifically stated, the mass of master link is equivalent to the mass of the master link plus that reassigned from the coupled driven link, which will be described later in this article. In Fig. 3, it was assumed that the driven link mass is evenly distributed among the master link and the moving platform [13]. The distance between the master link centroid a and the original centroid b is x .

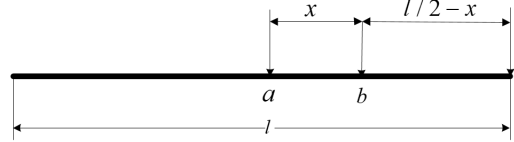


Fig. 3. Position of the master link centroid

The torque equilibrium, equation can be written as:

$$m_a g x - \frac{1}{2} m_s g (\frac{l}{2} - x) = 0 \quad (1)$$

and the centroid of the master link can be determined by:

$$l_c = x + \frac{1}{2}l = \frac{m_a + m_s}{2m_a + m_s}l \quad (2)$$

where m_a is the master link mass, m_s is the driven link mass, and l is the master length.

Then, the equivalent moment of inertia of the master link J_i and the moving platform J_m can be calculated. The original master link and driven link moment of inertia can be calculated as:

$$J_i = I_m + \frac{1}{3}m_a l^2 + \frac{1}{2}m_s l^2 \quad (3)$$

where I_m is the moment of inertia of the motor. The moment of inertia of the movable platform can be given as

$$J_m = R J_0 R^T = \begin{bmatrix} J_{mx} & J_{mxy} & J_{mxz} \\ J_{mxy} & J_{my} & J_{myz} \\ J_{mxz} & J_{myz} & J_{mz} \end{bmatrix} \quad (4)$$

As described in [14], the rotation matrix of the reference coordinate system O_BXYZ relative to coordinate system O_Dxyz can be given as

$$R = [U \ V \ W]^T \quad (5)$$

$J_0 = \text{diag} (J_{xx} \ J_{yy} \ J_{zz})$, where J_{xx} , J_{yy} and J_{zz} can be derived by:

$$\begin{cases} J_{xx} = \frac{1}{2}m_m r^2 + \frac{3}{4}m_s r^2 \\ J_{yy} = \frac{1}{2}m_m r^2 + \frac{3}{4}m_s r^2 \\ J_{zz} = m_m r^2 + \frac{3}{2}m_s r^2 \end{cases} \quad (6)$$

B. Jacobian Matrix and Dynamic Equation Solution

According to the previously established dynamic model of the 3-RSR SPW, a general expression based on the closed form of the joint space dynamics equation can be obtained [15]:

$$\tau = M(q)\ddot{q} + C(\dot{q}, q)\dot{q} + G(q) \quad (7)$$

For a system with N degrees of freedom, $M(q) \in \mathbb{R}^{N \times N}$ is the inertia matrix. $C(\dot{q}, q) \in \mathbb{R}^{N \times N}$ captures the Coriolis and centripetal effects, $G(q) \in \mathbb{R}^{N \times N}$ summarizes the gravity-related joint torques, and $\tau \in \mathbb{R}^{N \times N}$ are the joint torques of the driving the mechanism. In addition,

$q = [\alpha_{1a} \quad \alpha_{2a} \quad \alpha_{3a}]^T$ is the joint angle, \dot{q} is the joint velocity, and \ddot{q} is the joint acceleration. According to the simplified dynamic model, where the friction and elastic deformation of the mechanism are ignored, the dynamic equation can be described based on the virtual work principle:

$$\tau - J^T G_{move} - \tau_{GM} = (I_1 + I_2)\ddot{q} + J^T F_m \quad (8)$$

where τ is the motor torque, $F_m = m_j \ddot{X}$ is the moving platform inertia, J is the jacobian matrix of the mechanism, and $G_{move} = m_j [0 \quad 0 \quad -g]^T$ is the movable platform gravity, master link gravity torque can be calculated as:

$$\tau_{Gm} = m_i l_c g \begin{bmatrix} \cos \alpha_{1a} \\ \cos \alpha_{2a} \\ \cos \alpha_{3a} \end{bmatrix}. \quad (9)$$

Combining Eq. (3) and Eq. (4), the inertia matrices of the master link I_1 and driven link I_2 can be described by

$$I_1 = \begin{bmatrix} J_i & 0 & 0 \\ 0 & J_i & 0 \\ 0 & 0 & J_i \end{bmatrix}, I_2 = \begin{bmatrix} J_m & 0 & 0 \\ 0 & J_m & 0 \\ 0 & 0 & J_m \end{bmatrix} \quad (10)$$

The SPW can be considered as the relationship between the input coordinates (motor) and the output coordinates (moving platform) described by:

$$\dot{X} = J\dot{q} \quad (11)$$

where $\dot{X} = [\dot{x}_{OD} \quad \dot{y}_{OD} \quad \dot{z}_{OD}]^T$ is the velocity vector of the moving platform and $\dot{q} = [\dot{\alpha}_{1a} \quad \dot{\alpha}_{2a} \quad \dot{\alpha}_{3a}]^T$ is the velocity vector of the driving joint, if we take Eq. (11) with respect to time, we have:

$$\ddot{X} = J\ddot{q} + \dot{J}\dot{q} \quad (12)$$

substituting Eq. (12) into Eq. (8) we obtain

$$\tau = (I_1 + I_2 + m_j J^T J)\ddot{q} + J^T m_j \dot{J}\dot{q} + J^T G_{move} + \tau_{Gm} \quad (13)$$

Subsequently, the inertia matrix $M(q) \in \mathbb{R}^{N \times N}$, the Coriolis and centripetal matrix $C(\dot{q}, q) \in \mathbb{R}^{N \times N}$, and the gravity matrix $G(q) \in \mathbb{R}^{N \times N}$ can be obtained as followings:

$$\begin{cases} M(q) = I_1 + I_2 + m_j J^T J \\ C(\dot{q}, q) = J^T m_j \dot{J} \\ G(q) = J^T G_{move} + \tau_{Gm} \end{cases} \quad (14)$$

Based on Fig. 4, which illustrates a simplified branch, we can easily get $\|\overrightarrow{S_i O_D}\| = l$ ($i = 1, 2, 3$). If $a_i = \overrightarrow{S_i O_D}$, then

$$a_i^T a_i = l^2 (i = 1, 2, 3) \quad (15)$$

According to the geometric relationships [16], we can obtain:

$$a_i = \overrightarrow{O_B O_D} - \overrightarrow{O_B S_i} = \begin{bmatrix} x_{OD} \\ y_{OD} \\ z_{OD} \end{bmatrix} - T_i \begin{bmatrix} -l \cos \alpha_{ia} \\ 0 \\ -l \sin \alpha_{ia} \end{bmatrix} \quad (16)$$

$$T_i = \begin{bmatrix} \cos \beta_i & -\sin \beta_i & 0 \\ \sin \beta_i & \cos \beta_i & 0 \\ 0 & 0 & 1 \end{bmatrix} \quad (17)$$

where T_i is the rotation matrix, The revolute joint rotates by β_i around the $O_B z$ axis, where $\beta_i = (6 - 2i)\pi/3$, ($i = 1, 2, 3$).

If Eq. (15) is taken with respect to time $\dot{a}_i^T a_i + a_i^T \dot{a}_i = 0$. Due to that $\dot{a}_i^T a_i = a_i^T \dot{a}_i$, we can get:

$$\dot{a}_i^T a_i = 0 \quad (18)$$

$$\begin{aligned} \dot{a}_i &= \begin{bmatrix} \dot{x}_{OD} \\ \dot{y}_{OD} \\ \dot{z}_{OD} \end{bmatrix} - T_i \begin{bmatrix} \dot{x}_{OD} \\ \dot{y}_{OD} \\ \dot{z}_{OD} \end{bmatrix} (\dot{\alpha}_{ia}) \\ &= \dot{X} - b_i (\dot{\alpha}_{ia}) (i = 1, 2, 3) \end{aligned} \quad (19)$$

$$b_i = T_i \begin{bmatrix} l \sin \alpha_{ia} \\ 0 \\ l \cos \alpha_{ia} \end{bmatrix} \quad (20)$$

and according to Eq. (15), we can get:

$$\begin{aligned} &\begin{bmatrix} a_1^T \\ a_2^T \\ a_3^T \end{bmatrix} \dot{X} - \begin{bmatrix} a_1^T b_1 & 0 & 0 \\ 0 & a_2^T b_2 & 0 \\ 0 & 0 & a_3^T b_3 \end{bmatrix} \begin{bmatrix} \dot{\alpha}_{1a} \\ \dot{\alpha}_{2a} \\ \dot{\alpha}_{3a} \end{bmatrix} \\ &= \begin{bmatrix} 0 \\ 0 \\ 0 \end{bmatrix} \end{aligned} \quad (21)$$

$$\text{If } A = \begin{bmatrix} a_1^T \\ a_2^T \\ a_3^T \end{bmatrix} \text{ and } B = \begin{bmatrix} a_1^T b_1 & 0 & 0 \\ 0 & a_2^T b_2 & 0 \\ 0 & 0 & a_3^T b_3 \end{bmatrix} \text{ are}$$

constrained by the limitation of the spherical joint, $\overrightarrow{S_i O_D}$ is impossible to be in the same plane. Therefore a_1 , a_2 and a_3 are linearly independent, $[a_1 \quad a_2 \quad a_3]$ and A is reversible. The jacobian of the SPW can be obtained as:

$$J = A^{-1} B \quad (22)$$

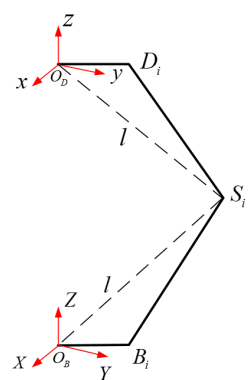


Fig. 4. Simplified branched-chain of the 3-RSR SPW

III. THE CONTROL SYSTEM STRUCTURE

It is known that the dynamic model is just an estimate of the actual model. On this basis, the computed torque decoupling control method with a traditional PD controller is introduced. After simulation, it was found that the above method was non-ideal, thus a fuzzy controller was added to change the computed torque decoupling control parameters with the traditional PD controller.

A. The Decoupling Control of Based on PD Controller

In the decoupling control scheme: a nonlinear compensator is introduced into the inner control loop [5], and the complex nonlinear strong-coupling system is transformed into an easy-to-control linear constant system [17]. As shown in Eq. (7), introduces the estimated control amount

$$\tau = \hat{M}(q)u + \hat{C}(\dot{q}, q)\dot{q} + \hat{G}(q) \quad (23)$$

where $\hat{M}(q)$ is an estimation of $M(q)$, $\hat{C}(\dot{q}, q)$ is an estimation of $C(\dot{q}, q)$, $\hat{G}(q)$ is an estimation of $G(q)$, and u is the input of the decoupling control system. We can get:

$$M(q)\ddot{q} + C(\dot{q}, q)\dot{q} + G(q) = \hat{M}(q)u + \hat{C}(\dot{q}, q)\dot{q} + \hat{G}(q) \quad (24)$$

Due to that $M(q)$ is definite, it must have inverse matrix. Thus, we can get

$$\ddot{q} = [M(q)^{-1}\hat{M}]u + M(q)^{-1}P \quad (25)$$

where $P = \hat{C}(\dot{q}, q) - C(\dot{q}, q)]\dot{q} + \hat{G}(q) - G(q)$.

it proved that under ideal and non-ideal conditions, the proposed decoupling control is stable.

a) Ideal

$\hat{C}(\dot{q}, q) = C(\dot{q}, q)$, $\hat{G}(q) = G(q)$, $\hat{M}(q) = M(q)$. In this case, the strong coupling nonlinear control system of the mechanism becomes a linear system of unit mass. Therefore,

$$\ddot{q} = u \quad (26)$$

When the expected trajectory is determined, we can get $\dot{q}_d(t)$ and $\ddot{q}_d(t)$, linear systems that can be used for the above unit mass Introduction of PD control with bias:

$$u = \ddot{q}_d + K_D(\dot{q}_d - \dot{q}) + K_P(q_d - q) = \ddot{q}_d + K_D\dot{e} + K_P e \quad (27)$$

where K_P and K_D are positive definite matrices, e is the position error, and \dot{e} is the velocity error. Then, a closed-loop system equation can be obtained:

$$\ddot{e} + K_D\dot{e} + K_P e = 0 \quad (28)$$

It can be proven that: when K_P and K_D are positive definite matrices, $(e, \dot{e}) = (0, 0)$ is the equilibrium point of global asymptotic stability, which starts from any initial condition $(q_0, \dot{q}_0), (q_0, \dot{q}_0) \rightarrow (q_d, \dot{q}_d)$.

The Lyapunov function is $V = \frac{1}{2}\dot{e}^2 + \int_0^e K_P x dx$, and if it is taken with respect to time, then:

$$\begin{aligned} \dot{V} &= \dot{e}\ddot{e} + K_P e\dot{e} \\ &= -\dot{e}(K_D\dot{e} + K_P e) + K_P e\dot{e} = -K_D\dot{e}^2 \leq 0 \end{aligned} \quad (29)$$

If $\dot{V} = 0$, then $-K_D\dot{e}^2 = 0$, $\dot{e} = 0$ and $\ddot{e} = 0$. Combined Eq. (28), it can be obtained that $(e, \dot{e}) = (0, 0)$ is the global asymptotic stability equilibrium point.

b) Non-ideal

If $\varepsilon(t)$ is the existing error interference, Eq. (26) can be described by:

$$\ddot{q} = u + \varepsilon(t), \quad (30)$$

and the closed-loop system equations can be written as:

$$\ddot{e} + K_D\dot{e} + K_P e = 0 + \varepsilon(t) \quad (31)$$

where $|\varepsilon(t)| < m$ and m are a constant.

If the closed-loop system with disturbances Eq. (30) is stable, then e is constant and $\dot{e} = \ddot{e} = 0$. Therefore, Eq. (31) can be written as:

$$K_P e = \varepsilon(t) \quad (32)$$

$$e = K_P^{-1}\varepsilon(t) = \begin{bmatrix} K_{P1}^{-1} & 0 & 0 \\ 0 & K_{P2}^{-1} & 0 \\ 0 & 0 & K_{P3}^{-1} \end{bmatrix} \varepsilon(t) \quad (33)$$

If $\varepsilon(t)$ is boundedness, K_{P1} , K_{P2} and K_{P3} can be increased to get $e \rightarrow 0$. Hence, K_p can be appropriately increased to solve the tracking accuracy problem caused by the deviation in the SPW dynamic model.

The mechanism with the control can be described by:

$$\tau = \hat{M}(q)(\ddot{q}_d + K_D\dot{e} + K_P e) + \hat{C}(\dot{q}, q)\dot{q} + \hat{G}(q) \quad (34)$$

The control block diagram is presented in Fig. 5.

B. Decoupling Control of Based on self-adaption PD Controller

Fuzzy control is a nonlinear control method [18]. If the fuzzy controller is added on the decoupling control with PD controller, the decoupling control based on self-adaption PD controller can be obtained. The structure of this control system is show in Fig. 6. If the position deviation e and velocity deviation \dot{e} are the inputs of the fuzzy controller, and the parameters K_P and K_D are the output of the PD controller, then the parameter self-adaption can be achieved.

IV. SIMULATION

The geometric parameters of the SPW included a circumscribed circle radius of the moving platform and the base of $R = 0.02m$ and $r = 0.02m$, respectively, a master link length of $L_A = 0.1m$, and a driven link length of $L_B = 0.1m$. The

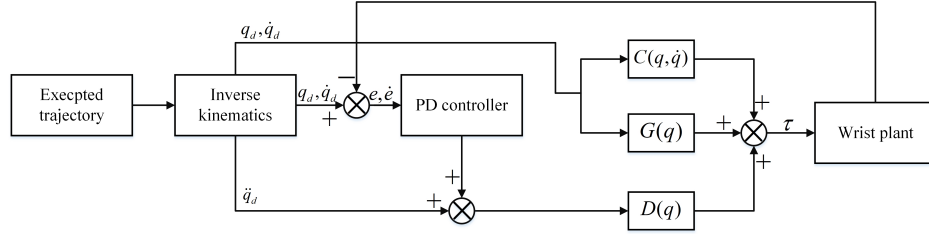


Fig. 5. The method of computed torque decoupling control with PD controller

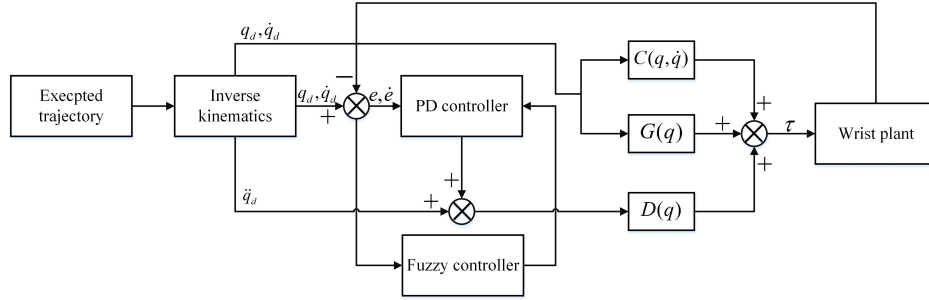


Fig. 6. The method of computed torque decoupling control with self-adaption PD controller

expected trajectory equation of the SPW robot is described by

$$\begin{cases} x = 50 \sin t \\ y = 50 \sin t \\ z = 0.2t^3 + t^2 + 80.19 \end{cases}, (0 \leq t \leq 5)$$

As it can be seen in Fig. 7 and Fig. 8, the effect of the 3-RSR SPW simulation with fuzzy-PD controller, included the effect of tracking and following error that was based on the fuzzy controller computed torque decoupling control.

As it can be seen in Fig. 9 and Fig. 10, the effect of the 3-RSR SPW computed torque decoupling control with PD controller, included the effect of tracking and tracking error.

As shown in Fig. 11 and Fig. 12, the change of K_P and K_D is expressed in fuzzy self-adaption.

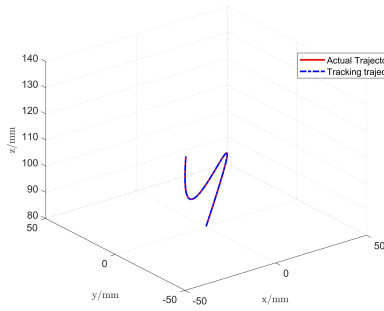


Fig. 7. The tracking effect of the 3-RSR SPW with fuzzy-PD controller

From the above results, it can be deduced that by adding a fuzzy-PD controller to the system, the K_D and K_P parameters undergo small changes, the tracking effect is significantly

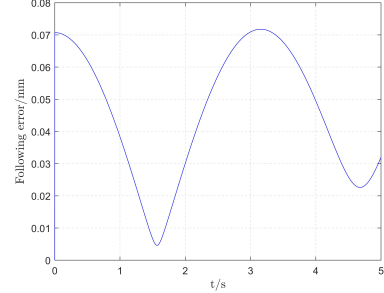


Fig. 8. The tracking error of the 3-RSR SPW with fuzzy-PD controller

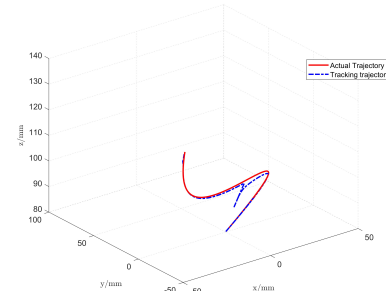


Fig. 9. The tracking effect of the 3-RSR SPW with PD controller

improved and quickly stabilized, and the tracking error is smaller.

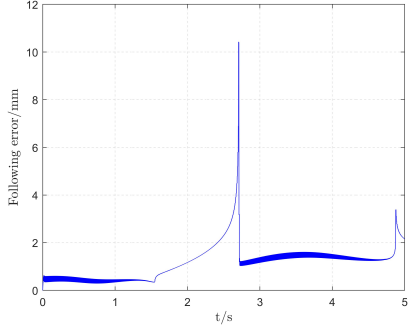


Fig. 10. The tracking error effect of the 3-RSR SPW with PD controller

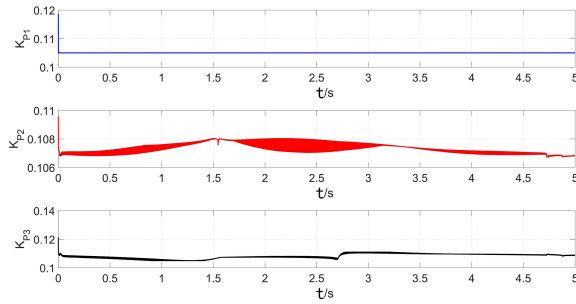


Fig. 11. The K_P parameters of the fuzzy controller

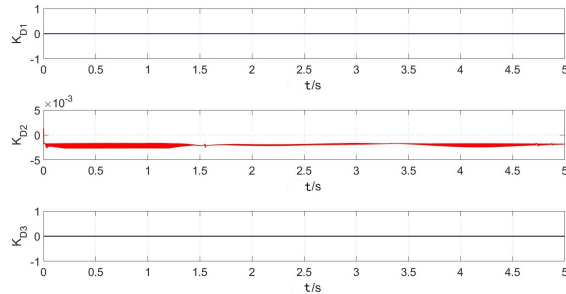


Fig. 12. The K_D parameters of the fuzzy controller

V. CONCLUSION

In this article a control strategy was proposed, which includes the computed torque decoupling control method with traditional PD controller and with self-adaption. It was proved that the dynamic of the robot is global asymptotic stable in the ideal and non-ideal estimation. According to the Adams-Matlab co-simulation, the control output results can be obtained, which indicate that the conclusion of the stability of the computed torque decoupling control system can be easily found, with a small control error. This work provides an important theoretical basis for the subsequent improvement of the robots dynamic tracking and control performance.

REFERENCES

- [1] Uchiyama M. A new design of a very fast 6-DOF parallel robot[C]. Proc. 23rd Int. Symp. Industrial Robots, 1992: 771-776.
- [2] Kang B, Chu J, Mills J K. Design of high speed planar parallel manipulator and multiple simultaneous specification control[C]. Robotics and Automation, 2001. Proceedings 2001 ICRA. IEEE International Conference on. IEEE, 2001, 3: 2723-2728.
- [3] Gosselin C, Angeles J. The optimum kinematic design of a planar three-degree-of-freedom parallel manipulator[J]. Journal of mechanisms, transmissions, and automation in design, 1988, 110(1): 35-41.
- [4] ZHANG Guoying, LIAO Yajun, LIANG Feng, SU Manjia, GUAN Yisheng, LIU Guanfeng, CHEN Xin. A Spheroid Parallel Wrist Mechanism and Its Kinematic Analysis. ROBOT, 2017, 39(2): 167-175.
- [5] CHEN Weinan, LIU Guanfeng, LIN Xieyuan, ZHANG Guoying, GUAN Yisheng. Decoupling Control and Simulation of a 2-DOF Parallel Robot[J]. Journal of Mechanical Engineering, 2015, 51(13): 152-157.
- [6] Ouyang P R, Zhang W J, Wu F X. Nonlinear PD control for trajectory tracking with consideration of the design for control methodology[C]. Robotics and Automation, 2002. Proceedings. ICRA'02. IEEE International Conference on. IEEE, 2002, 4: 4126-4131.
- [7] Nguyen C C, Antrazi S S, Zhou Z L, et al. Adaptive control of a Stewart platform-based manipulator[J]. Journal of Robotic systems, 1993, 10(5): 657-687.
- [8] Wang H, Xue C, Gruver W A. Neural network control of a parallel robot[C]. Systems, Man and Cybernetics, 1995. Intelligent Systems for the 21st Century. IEEE International Conference on. IEEE, 1995, 3: 2934-2938.
- [9] Ren L, Mills J K, Sun D. Controller design applied to planar parallel manipulators for trajectory tracking control[C]. Robotics and Automation, 2005. ICRA 2005. Proceedings of the 2005 IEEE International Conference on. IEEE, 2005: 968-973.
- [10] Su Y, Sun D, Ren L, et al. Integration of saturated PI synchronous control and PD feedback for control of parallel manipulators[J]. IEEE Transactions on Robotics, 2006, 22(1): 202-207.
- [11] Codourey A. Dynamic modeling of parallel robots for computed-torque control implementation[J]. The International Journal of Robotics Research, 1998, 17(12): 1325-1336.
- [12] Codourey A. Dynamic modelling and mass matrix evaluation of the DELTA parallel robot for axes decoupling control[C]//Intelligent Robots and Systems' 96, IROS 96, Proceedings of the 1996 IEEE/RSJ International Conference on. IEEE, 1996, 3: 1211-1218.
- [13] Gallot G, Ibrahim O, Khalil W. Dynamic modeling and simulation of a 3-d hybrid structure eel-like robot[C]//Robotics and Automation, 2007 IEEE International Conference on. IEEE, 2007: 1486-1491.
- [14] Guo-ying Z, Hao J, Tao Z, Cai X, Guan-feng L, Xiao-lan X, Shao-ming L. Dynamic Modeling and Analysis of 3-DOF Spheroid Parallel Mechanism[J]. Journal of Guangdong University of Technology, 2018, 6(35): 24-30.
- [15] Carp-Ciocardia D C. Dynamic analysis of Clavel's Delta parallel robot[C]//Robotics and Automation, 2003. Proceedings. ICRA'03. IEEE International Conference on. IEEE, 2003, 3: 4116-4121.
- [16] Pierrot F, Fournier A, Dauchex P. Towards a fully-parallel 6 dof robot for high-speed applications[C]//Robotics and Automation, 1991. Proceedings., 1991 IEEE International Conference on. IEEE, 1991: 1288-1293.
- [17] Di Gregorio R. Kinematics of the 3-RSR Wrist[J]. IEEE transactions on robotics, 2004, 20(4): 750-753.
- [18] Qiao W Z, Mizumoto M. PID type fuzzy controller and parameters adaptive method[J]. Fuzzy sets and systems, 1996, 78(1): 23-35.